

A fretting test apparatus for measuring friction hysteresis of bolted joints

*Original*

A fretting test apparatus for measuring friction hysteresis of bolted joints / Li, D., Xu, C., Botto, D., Zhang, Z., Gola, M.. - In: TRIBOLOGY INTERNATIONAL. - ISSN 0301-679X. - ELETTRONICO. - 151:(2020), p. 106431. [10.1016/j.triboint.2020.106431]

*Availability:*

This version is available at: 11583/2838299 since: 2020-07-07T22:55:56Z

*Publisher:*

Elsevier

*Published*

DOI:10.1016/j.triboint.2020.106431

*Terms of use:*

This article is made available under terms and conditions as specified in the corresponding bibliographic description in the repository

*Publisher copyright*

Elsevier postprint/Author's Accepted Manuscript

© 2020. This manuscript version is made available under the CC-BY-NC-ND 4.0 license <http://creativecommons.org/licenses/by-nc-nd/4.0/>. The final authenticated version is available online at: <http://dx.doi.org/10.1016/j.triboint.2020.106431>

(Article begins on next page)

# A fretting test apparatus for measuring friction hysteresis of bolted joints

Dongwu Li<sup>1</sup>, Chao Xu<sup>1,2\*</sup>, Daniele Botto<sup>3</sup>, Zhishu Zhang<sup>1</sup>, Muzio Gola<sup>3</sup>

<sup>1</sup>*School of Astronautics, Northwestern Polytechnical University, Xi'an 710072, China*

<sup>2</sup>*Qingdao R&D Institute, Northwestern Polytechnical University, Qingdao, 266200, China*

<sup>3</sup>*Department of Mechanical and Aerospace Engineering, Politecnico di Torino, Turin 10129, Italy*

**Abstract:** This paper focuses on an experimental investigation of the mechanical behavior of bolted joints. A new test apparatus to measure friction hysteresis was designed to provide a reliable experimental database for the calibration of contact models. This apparatus uses a piezoelectric actuator to provide the contact interfaces with stable oscillatory relative displacement. The friction force and the bolt preload were continuously measured during the test, using a load cell and a force washer, respectively. The relative motion between the interfaces was measured using a single laser vibrometer. The influence of the bolt preload and excitation amplitude on friction hysteresis was investigated. A numerical model was developed to extract the tangential contact stiffness from the measured data.

**Keywords:** Fretting tests; bolted joints; friction hysteresis; contact stiffness.

---

\* Corresponding author: [chao\\_xu@nwpu.edu.cn](mailto:chao_xu@nwpu.edu.cn)  
Address: No.127 Youyi Road, Xi'an, Shaanxi 710072, China

# 1 Introduction

Several mechanical assemblies use bolted joints. A significant advantage of bolted joints is that they can be easily assembled and disassembled. When a joint undergoes oscillatory loads the contact interfaces experience a relative motion. Friction forces induced by this relative motion exhibit nonlinear behavior with hysteresis. Different regimes can be observed during oscillatory motion [1]. In the stick regime, the relative displacement between the contact surfaces is very small and the tangential force depends almost linearly on the relative displacement. In the gross-slip regime, displacements are large and the tangential force is saturated to the maximum friction force. The transition between the stick and the gross-slip regime is denoted as microslip. The tangential force does not vary linearly with displacement and is lower than the maximum friction force.

Hysteresis depends on contact conditions, affects the dynamic behavior of the joint and results in energy dissipation [2]. Hysteresis loops, namely the tangential friction force as a function of the relative displacement, can be replaced with a simplified model of friction contact [3-6]. These friction models can be combined with dynamic analysis to simulate the nonlinear dynamics of structures with bolted joints. In these models, two major issues need to be addressed: (i) the accurate reproduction of the friction nonlinear behavior, and (ii) a precise calculation of contact parameters (tangential contact stiffness and friction coefficient). A good calibration of these contact models depends on accurate measurement of the hysteresis loops using precisely controlled experiments. In this way, the development of an innovative experimental technique can advance understanding of the behavior of

36 the bolted joint interfaces. Consequently, more reliable models can be used to simulate the nonlinear  
2  
3  
37 dynamics of bolted joint structures.  
4  
5

6  
7  
8  
39 Previous experimental research on the nonlinear behavior of bolted joints has determined damping  
10  
11  
12  
40 characteristics through the structural dynamic response [7-9]. Interface damping is often identified  
13  
14  
15  
41 according to the experimental frequency response functions. More recently, an experimental  
16  
17  
18  
42 investigation into friction damping has focused on the direct measurement of friction behavior. Gaul et  
19  
20  
21  
43 al. [10, 11] developed an experimental setup to measure the response functions and the damping  
22  
23  
24  
44 characteristics of a bolted joint placed between two lumped masses. This setup is a resonator in which  
25  
26  
27  
45 the relative motion between joint interfaces is excited by its longitudinal vibration mode. The inertia  
28  
29  
30  
46 force of the free end mass is regarded as the tangential friction force transmitted over the joint interface.  
31  
32  
33  
47 Sandia National Laboratories [12] utilized a similar idea and proposed a resonant apparatus. In these  
34  
35  
36  
48 two experimental devices, the excitation imposed by electromagnetic shakers cannot excite any  
37  
38  
39  
49 vibration modes other than the desired longitudinal mode. Abad et al. [13, 14] did experiments to  
40  
41  
42  
50 study the friction behavior of bolted joints with a quasi-static excitation imposed by a universal testing  
43  
44  
45  
51 machine. Eriten et al. [15] developed a lap joint fretting apparatus to measure hysteresis loops and  
46  
47  
48  
52 contact parameters of bolted joints and studied the influence of normal preload, maximum tangential  
49  
50  
51  
53 displacement, and material on the joint parameters. This apparatus employs a piezoelectric actuator  
52  
53  
54  
54 with a closed-loop control to provide oscillatory motions of the lap joint. Also, some researchers [16,  
55  
56  
57  
55 17] have performed experiments on the interface friction behavior of bolted joints under torsional  
56  
57  
58  
56 loading. In [16] it was found that decreasing the bolt preload the hysteresis loop changed from an  
59  
60  
61  
62  
63  
64  
65

57 elliptical shape to a distorted four-sided polygon. Increasing the angular amplitude, the hysteresis  
2  
3  
58 loops became shaped like parallel hexagons. This behavior was explained by the authors as being  
5  
69 caused by the relative slippage between the contact threads [17].  
8

80  
10  
11  
12  
13  
14  
15  
16  
17  
18  
19  
20  
21  
22  
23  
24  
25  
26  
27  
28  
29  
30  
31  
32  
33  
34  
35  
36  
37  
38  
39  
40  
41  
42  
43  
44  
45  
46  
47  
48  
49  
50  
51  
52  
53  
54  
55  
56  
57  
58  
59  
60  
61  
62  
63  
64  
65

In general, three variables need to be measured in fretting friction experiments, i.e. the tangential friction force, the tangential relative displacement between contact surfaces, and the normal preload. Contact stiffness, namely the slope of the hysteresis loop at the stick stage, and the friction coefficient, that is the ratio of the tangential force over the normal preload at the gross-slip stage, can both be extracted by the variables measured.

The tangential relative displacement is generally very small, less than 100 microns, and requires a very accurate measurement method. Gaul et al. [10, 11] and Sandia National Laboratories [12] used frequency domain integration techniques to obtain the tangential displacement from measured acceleration data. However, the inevitable noise in measured data may introduce errors in the integration process. In [10-12] the tangential friction force was measured with an accelerometer located on the lumped mass at the remote end of the shaker. Kartal et al. [18] employed Digital Image Correlation (DIC) to determine the relative displacement of the contact interfaces. The accuracy of the measured displacement largely depends on the resolution and size of the selected images. Eriten et al. [15] employed a single Laser Nano Sensor and a small mirror to measure the tangential displacement of the joint specimen at the moving end. However, the motion of the specimen at the fixed end was considered negligible assuming high rigidity at that location. The tangential friction force was

78 measured with a tri-axial load cell which allows for monitoring a possible misalignment in  
2  
3  
49 out-of-plane directions. Schwingshackl et al. [19] developed the “Imperial College London”  
5  
6  
70 first-generation friction apparatus. This apparatus utilizes a single Laser Doppler Vibrometer (LDV) to  
8  
9  
81 measure the displacement of the moving contact surface. Also, in this case, the displacement was  
10  
11  
12  
13  
14  
15  
16  
17  
18  
19  
20  
21  
22  
23  
24  
25  
26  
27  
28  
29  
30  
31  
32  
33  
34  
35  
36  
37  
38  
39  
40  
41  
42  
43  
44  
45  
46  
47  
48  
49  
50  
51  
52  
53  
54  
55  
56  
57  
58  
59  
60  
61  
62  
63  
64  
65

87 The accuracy of the estimated friction coefficients heavily depends on the precision of bolt preload.  
88 In [15, 27], the bolt preload was determined by a torque-preload relationship with torque-controlled  
89 measurements. The calculated preload may be inaccurate because this relationship depends on the  
90 friction coefficient [14], which is known only approximately. Li et al [26] used a strain gauge glued to  
91 the bolt to measure the axial deformation of the bolt and therefore the corresponding preload. Abad et  
92 al. [13] used an annulus force washer to measure the bolt preload in their test device.

94 This paper describes a fretting test apparatus purposely developed to investigate the friction behavior  
95 of bolted joints and estimate the contact parameters. The tangential friction force is measured with a  
96 dynamic load cell, while a single LDV in combination with a prism measures the relative  
97 displacement and the bolt preload is detected by a force washer. This apparatus can also be employed  
98 to study the effect of fretting wear on the contact parameters.

99  
100  
101  
102  
103  
104  
105  
106  
107  
108  
109  
110  
111  
112  
113  
114  
115  
116  
117  
118  
119  
120  
121  
122  
123  
124  
125  
126  
127  
128  
129  
130  
131  
132  
133  
134  
135  
136  
137  
138  
139  
140  
141  
142  
143  
144  
145  
146  
147  
148  
149  
150  
151  
152  
153  
154  
155  
156  
157  
158  
159  
160  
161  
162  
163  
164  
165

The paper is organized as follows. [Section 2](#) describes the developed test apparatus and introduces the measurement method of hysteresis loops in detail. [Section 3](#) analyses the repeatability of test results and the effect of bolt preload, and excitation amplitude on measured hysteresis loops and contact parameters. [Section 4](#) models the contact between the bolted joint to simulate the tangential force/relative displacement relationship. Results from the numerical simulation are validated with the measured data. [Section 5](#) highlights the accuracy and reliability of the test apparatus.

## 2 Experimental apparatus

### 2.1 Description of the test apparatus

An overall view of the rig is depicted in [Fig. 1](#). A leaf spring (7) is clamped between two C-shaped half-frames (5) and (12) by tightening two bolts (1). The two half-frames are machined from a monolithic steel block and make up the frame of the rig. The frame forms an O-shaped closed gate so that all the internal forces are self-balanced. A piezoelectric actuator (17) is connected to the left side of the leaf spring. The actuator displaces the leaf spring with an oscillating motion that is transmitted to a moving specimen (15). The moving specimen is connected to the right side of the leaf spring with two M6 bolts (8). A fixed specimen (10) is attached to one end of the load cell (13). The other end of the load cell is borne by the right support of the frame. The contact surfaces of the moving and fixed specimens are brought into contact with a M6 bolt (14). A force washer (9) is used to measure the bolt preload and to monitor its variation in real-time. The relative displacement between the fixed and moving specimens is measured using a laser vibrometer, as shown in [Fig. 2](#). The contact surfaces and the axis of the load cell are carefully aligned so that the load cell measures the tangential contact force with great accuracy. The test apparatus is placed on an optical vibration isolation table to reduce the effects of external vibrations on the measurements. Specimens can be assembled without disassembling the excitation system, which greatly reduces the overall assembly time (no more than 20 minutes).

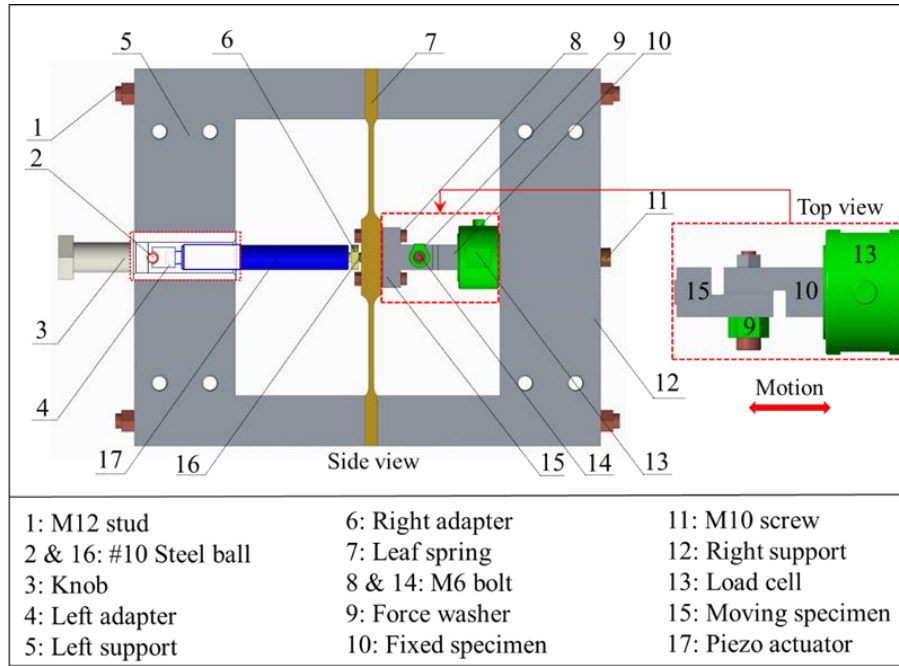


**Fig. 1.** Sketch of the developed test apparatus and main components.

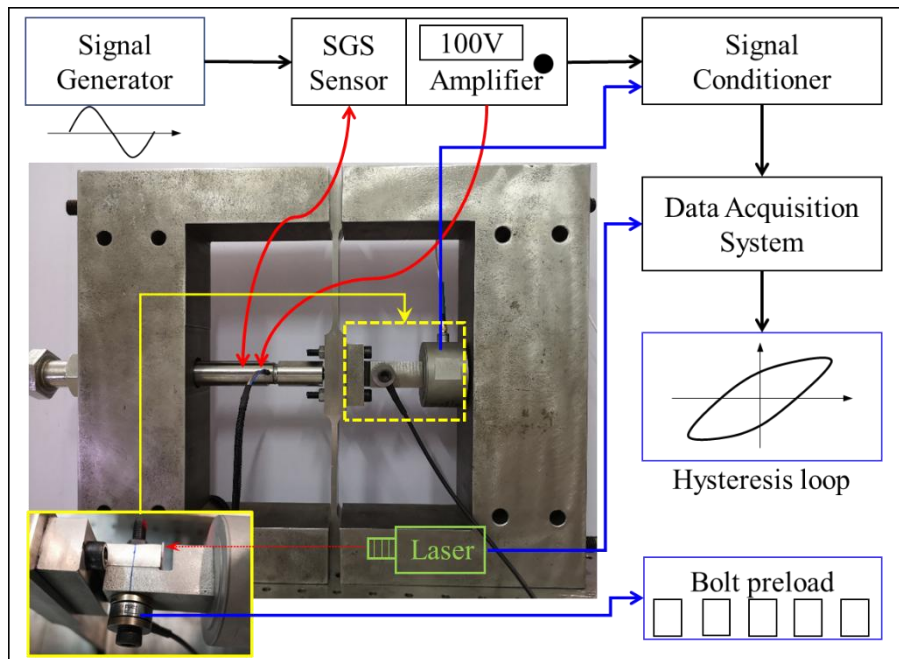


**Fig. 2.** Photograph of the test apparatus and details of the measuring system.

The fretting test apparatus consists of three subassemblies, namely the excitation system, the measurement system and the specimens, that are described in the following.

132  
2  
3  
133  
4  
5  
6  
134  
7  
8  
9  
135  
10  
11  
12  
136  
13  
14  
15  
137  
16  
17  
18  
138  
19  
20  
21  
139  
22  
23  
140  
24  
25  
26  
141  
27  
28  
29  
142  
30  
31  
32  
143  
33  
34  
35  
144  
36  
37  
38  
145  
39  
40  
41  
146  
42  
43  
44  
147  
45  
46  
47  
148  
48  
49  
50  
51  
52  
53  
54  
55  
149  
56  
57  
58  
59  
60  
61  
62  
63  
64  
65

## 2.2 Excitation system

The excitation system consists of a piezoelectric actuator (17), driven by a signal generator and a power amplifier. The piezoelectric actuator (PSt150/14/100VS20, Coremorrow Inc.) is preloaded. The piezoelectric actuator is closed-loop controlled by a servo controller (E-509.x1, Physik Instrument Inc.) through an integrated position feedback sensor. In the fretting rig the controlled variable should be the relative displacement between the contact surfaces but this closed-loop control has not been implemented yet. The actuator was driven using its calibration curve that gives the relationship between the displacement of the actuator and the input voltage. Piezoelectric actuators cannot be loaded with shear forces that could lead to a premature failure. Therefore, an uncoupling system has been devised. This uncoupling system consists of two adapters (4) and (6) placed at both ends of the actuator, as shown in Fig. 3. A steel sphere (16) is located between the adapter (4) and the leaf spring, while another steel sphere is located between the adapter (6) and the knob (3). Both spheres are embedded in spherical grooves. The point contact transmits normal load, but it cannot transmit shear or bending loads. A preload is applied by screwing the knob to avoid losing contact between the spheres and their counterparts. The magnitude of this preload does not affect the measured results.

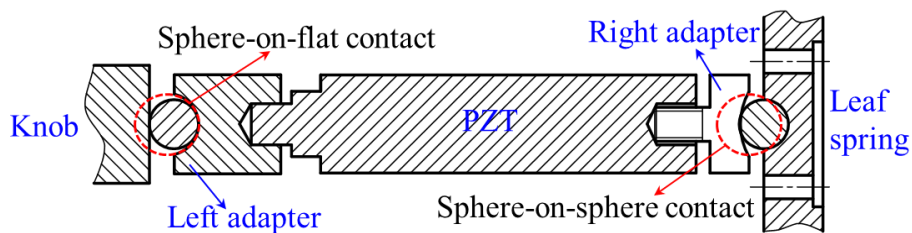
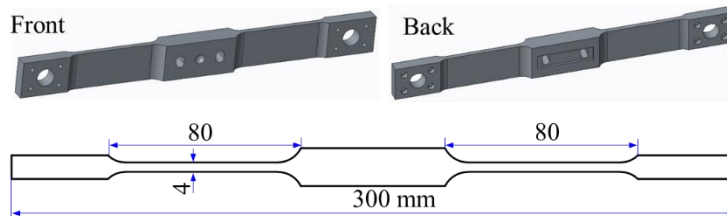


Fig. 3. Scheme for protecting the piezoelectric actuator.

151  
2  
3  
152  
5  
6  
153  
8  
9  
154  
10  
11  
155  
13  
14  
156  
16  
17  
157  
19  
20  
158  
22  
23  
159  
25  
26  
160  
27  
28  
161  
30  
31  
32  
162  
33  
34  
35  
36  
37  
38  
39  
40  
41  
163  
42  
43  
44  
164  
45  
46  
165  
48  
49  
166  
51  
52  
167  
53  
54  
55  
168  
56  
57  
169  
59  
60  
61  
62  
63  
64  
65

If the actuator is displaced along the transverse direction the contact angle between the sphere and the groove changes and gives a counter-reaction. This counter-reaction, that is opposite to the displacement, is enough to keep the piezoelectric in the right position if the transverse displacement is small. The leaf spring, see Fig. 4, drives the longitudinal motion and minimizes the transverse displacement. To avoid resonances the leaf spring was designed so that its natural frequencies are higher than the operating frequency of the rig. However, the leaf spring cannot be too stiff, because in that case the actuator is not able to displace the moving specimen up to the gross-slip regime. Therefore, the leaf spring was designed with a stiffness equal to 5% of the actuator stiffness (40 kN/mm) and with a first natural frequency of about 215 Hz. The overall resonance of the rig is far from the nominal operating frequency (25 Hz) and the leaf spring is soft enough to allow the piezoelectric actuator to displace the moving specimens up to gross-slip regime.



**Fig. 4.** Sketch of the leaf spring and schematic of the front and back sides.

### 2.3 Measurement system

A dynamic load cell (1061V2, Dytran Instruments Inc., full-scale  $\pm 2224$  N with 2.25 mV/N sensitivity) measures the tangential friction force. A force washer (KMR/20 kN for M6 bolt, HBM Inc., 1.7 mV/V sensitivity) measures the bolt preload. A DC power supply (GPD-3303S, GW Instek Inc.) feeds the force washer with 2.5 V DC voltage. A high-precision 5.5-digit digital multimeter

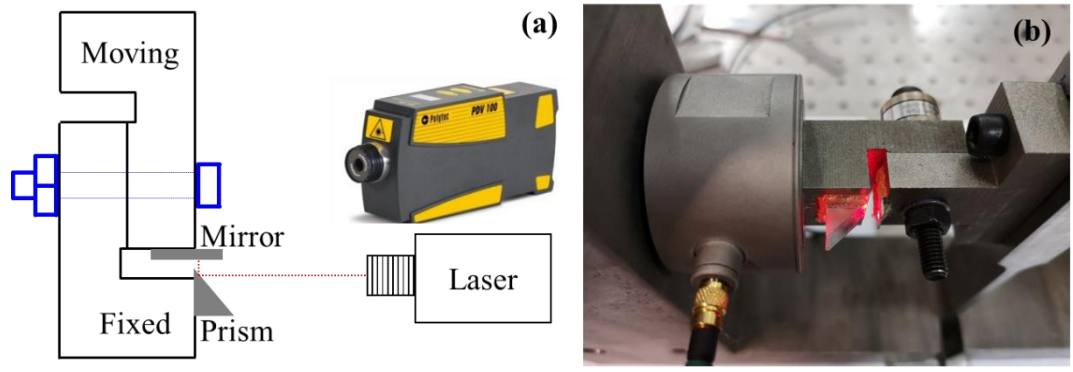
170 (34450A, Keysight Technologies Inc.) measures in real-time the output voltage of the force washer.

2  
3  
171 4  
5  
6  
172 Test rigs that use a single LDV assume that the fixed specimen has a negligible motion [15, 19].

8  
9  
173 However, the fixed specimen is a deformable body that undergoes displacements under the tangential  
10  
11  
174 friction force. For this reason, two LDVs are usually used in test rigs found in the literature [21, 22].  
12  
13

14  
15  
175 Section 3 shows some measurements that emphasize the difference between the relative and absolute  
16  
17  
176 displacements. In this test rig the true relative displacement is measured by using a single LDV and a  
18  
19  
20  
177 prism without any approximation.  
21  
22

23  
178 24  
25  
26  
179 Figure 5(a) depicts the schematic of the original technique adopted in this work. The laser beam is  
27  
28  
29  
180 reflected by means of a prism on the target measurement point. This prism (size 10×10×10 mm) is  
30  
31  
32  
181 attached to the fixed specimen while a small mirror (size 10×5 mm) is attached to the moving  
33  
34  
35  
182 specimen. Figure 5(b) shows their positions on the specimens. The prism and the mirror are light and  
36  
37  
38  
183 small, so they do not affect the measurements.  
39



184  
185 **Fig. 5.** (a) Schematic of the measurement method of relative displacement between fixed and moving  
186 specimens, (b) Installation location of the prism and the mirror.  
58  
59  
60  
61  
62  
63  
64  
65

187  
2  
3  
188  
4  
5  
189  
6  
7  
8  
190  
9  
10  
11  
12  
191  
13  
14  
15  
16  
17  
192  
18  
19  
20  
194  
21  
22  
23  
195  
24  
25  
26  
27  
28  
29  
196  
30  
31  
32  
33  
34  
197  
35  
36  
37  
38  
39  
40  
41  
42  
43  
198  
44  
45  
46  
199  
47  
48  
49  
200  
50  
51  
52  
53  
54  
55  
201  
56  
57  
202  
58  
59  
60  
61  
62  
63  
64  
65

The method to measure the relative displacement using only one laser beam is detailed in principle as follows. In Fig. 6 points B' and B represent the position of the moving specimen at initial time  $t_1$  and final time  $t_2$  respectively. Under the friction force the fixed specimen moves and the laser spot on the prism, that is attached to the fixed specimen, changes from A' to A. The solid blue line boxes and the green dotted line boxes represent the positions of the moving and fixed specimens at time  $t_1$  and  $t_2$ . The displacements of the moving and fixed specimens during the time interval  $\Delta t = t_2 - t_1$  are  $u_M$  and  $u_F$  respectively. The relative displacement is then  $\delta = |u_F - u_M|$ . At time  $t_1$  the distance between the laser head and the mirror on the moving sample is,

$$d_{t_1} = |OA'| + |A'B'|. \quad (1)$$

At time  $t_2$  the distance becomes

$$d_{t_2} = |OA| + |AB|, \quad (2)$$

where

$$|OA| = |OA'| + u_F \tan(\alpha), \quad (3)$$

$$|AB| = |A'B'| - u_M,$$

and  $\alpha$  is the  $45^\circ$  angle of the prism. Substituting Eq. (3) into Eq. (2) yields the distance at time  $t_2$ ,  $d_{t_2} = |OA'| + |A'B'| + u_F - u_M$ . Therefore, the displacement measurement by the laser beam within a time interval  $\Delta t$  is

$$|d_{t_2} - d_{t_1}| = |u_F - u_M| = \delta. \quad (4)$$

Equation (4) demonstrates that the relative displacement  $\delta$  can be measured with a single beam and a prism inclined of  $45^\circ$  relative to the direction measured motion.

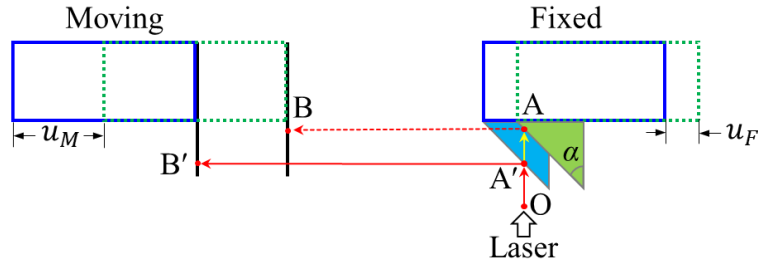


**Fig. 6.** Principle of relative displacement measurement method using a single head laser.

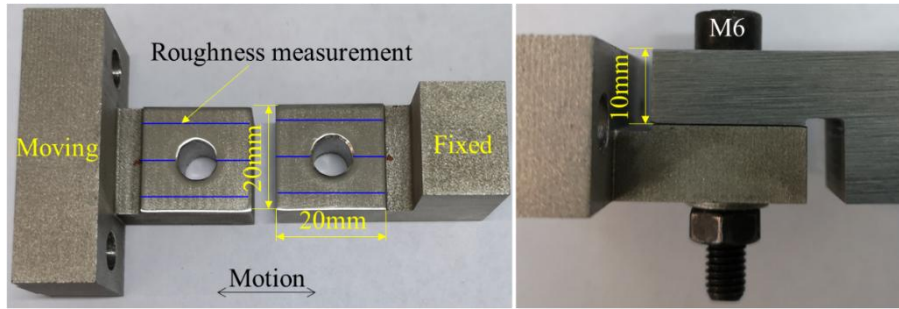
The laser beam needed to be carefully adjusted before each test to ensure that it makes an angle of  $45^\circ$  to the bevel of the prism. Moreover, the reflection point of the laser beam was focused as close as possible to the surface of the joints. The prism and the mirror were glued using a layer of evenly distributed Petro wax to make the reflectors firm and easy to disassemble. Moreover, the periphery of the reflectors was wrapped with hot melt adhesive, as shown in Fig. 5(b), to reduce vibrations.

Friction force and displacements were acquired with a 16-bit data acquisition board (PCI-6251, National Instruments Inc.) and an in-house code. Signals were conditioned with a 12-channel signal conditioner (YE3826A, Sinocer Inc.) before acquisition. Displacement of the actuator tip was also acquired to monitor the stability of the device. Output force and displacement signals were sampled at 5 kHz with no filtering.

## 2.4 Bolted joint specimen

The bolted joint specimens under tests were made of ASTM 304 stainless steel with a yield strength of 215 MPa. The tested bolts are M6, carbon steel, class 8.8. The potential contact region is a  $20 \times 20$  mm square with a 7 mm diameter through-hole, see Fig. 7. Before the tests, all samples and bolts were

221 cleaned with alcohol in an ultrasonic cleaner for 30 min to avoid the influence of particles and  
2 machine oil, then dried to ensure dry friction conditions. To reduce the impact of the bolted joint  
222 assembly error on the experimental results, a feeler gauge was used to ensure that the two  
5  
223 through-holes were as coaxial as possible.  
8  
224



225  
22  
23  
226 **Fig. 7.** Photograph of the bolted joint specimen.  
25

26  
227  
28  
228 The specimens were machined by wire cutting. Then the contact surfaces were carefully  
30  
229 hand-polished using two different grades of sandpaper (first 800 grit and then 1200 grit). The  
33  
34  
230 roughness  $R_a$  of the contact surfaces of the joint samples was measured using a portable roughness  
36  
37  
231 profilometer (TR200, Jitai Keyi Inc.). The selected measurement positions are shown in the blue line  
39  
40  
232 in Fig. 7(a). The test length along each long blue line segment is 4 mm, and that along each short  
42  
43  
233 blue line segment is 2.4 mm. The average value of the roughness of each line segment is regarded as  
45  
46  
234 the roughness of the contact surface. The roughness of the contact surfaces of the moving and fixed  
48  
49  
235 specimens used in the tests are  $0.78 \mu\text{m}$  and  $0.91 \mu\text{m}$ , respectively. All tests were conducted at  
51  
52  
236 room temperature.  
53

### 3 Experimental results and discussion

The tangential force as a function of displacement gives the hysteresis loop which represents the nonlinear characteristics of the joint interface. The area enclosed by the hysteresis loop represents dissipated energy per cycle. Figure 8 shows a typical hysteresis loop obtained with this test apparatus. The loop shows the three fretting regimes. During the stick regime, the force varies linearly with the relative displacement and only elastic deformation occurs on the contact surface. Increasing the relative displacement until the whole contact area is slipping gives the gross-slip regime. In this regime the tangential force reaches its maximum value. The transition between stick and gross-slip regimes is the microslip regime, in which a portion of the contact area is sliding whereas the other portion is still stuck.

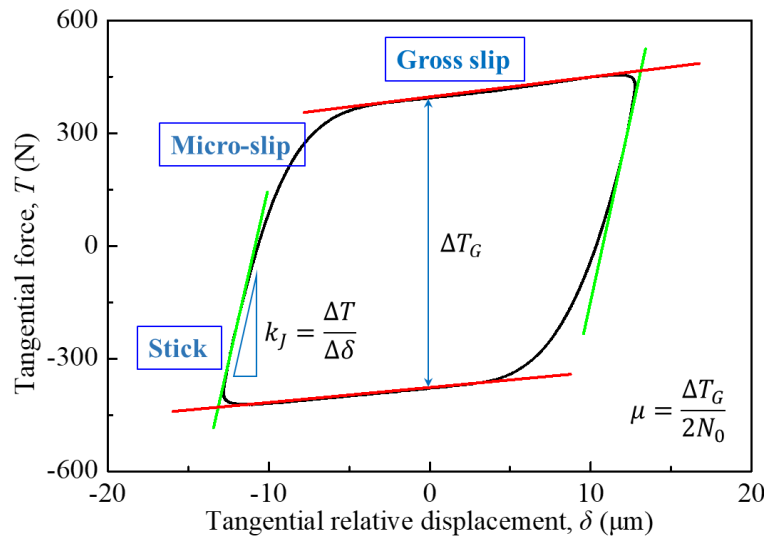


**Fig. 8.** Typical hysteresis loop and schematic of the extraction of contact parameters (stiffness and friction coefficient).

The hysteresis loop can be characterized by three contact parameters: bolt preload  $N_0$ , tangential

252 contact stiffness  $k_J$ , and friction coefficient  $\mu$ . The bolt preload is measured with the force washer.  
2  
253 The tangential contact stiffness is defined as the slope of the hysteresis loop at the stick stage. In this  
5  
254 paper, it was determined with the ratio of the force/displacement increments  $k_J = \Delta T / \Delta \delta$ , as shown in  
8  
255 Fig. 8. The increments  $\Delta T$  and  $\Delta \delta$  were set by choosing 120 points within the linear portion of the  
10  
256 loop at the reversal. It should be noted that between the fixed and the moving contact surfaces of the  
13  
14  
257 joint there are other deformability sources due to the interfaces at the washer, at the screw head and at  
16  
17  
258 the nut. Moreover, also the bolt shank contributes with its elasticity. A simplified model of the joint in  
19  
20  
259 Fig. 16 helps in visualizing the various stiffness sources. A more detailed analysis of these stiffness  
22  
23  
260 values will be given in section 4. Therefore, the measured tangential stiffness  $k_J$  is the overall joint  
25  
261 stiffness and the contact stiffness  $k_t$  of the target surface will be inferred by  $k_J$ . The friction  
27  
28  
262 coefficient is defined as the ratio of the tangential force  $T_G$  over the normal force  $N_0$  during the  
30  
31  
263 gross slip stage,  $\mu = T_G / N_0$ . In these experiments, the tangential force during the gross-slip stage  
33  
34  
264 was not constant but it slightly increased with the displacement, see the red line in Fig. 8. The  
36  
37  
265 displacement-force relationship can be characterized by a linear residual stiffness, and the friction  
39  
40  
266 coefficient was estimated by the ratio of the distance between two red lines in Fig. 8 over twice the  
42  
43  
267 bolt preload [19],  $\mu = \Delta T_G / 2N_0$ .

45  
46  
268  
48  
49  
269 Figure 9 shows two measured hysteresis loops, under the same operating conditions, plotted using  
51  
52  
270 the absolute displacement and the relative displacement. The absolute displacement was measured on  
53  
54  
271 the moving specimen fixing the prism to the optical table. As expected, the relative displacement was  
56  
57  
272 noticeably lower, about 40%, than the absolute displacement.

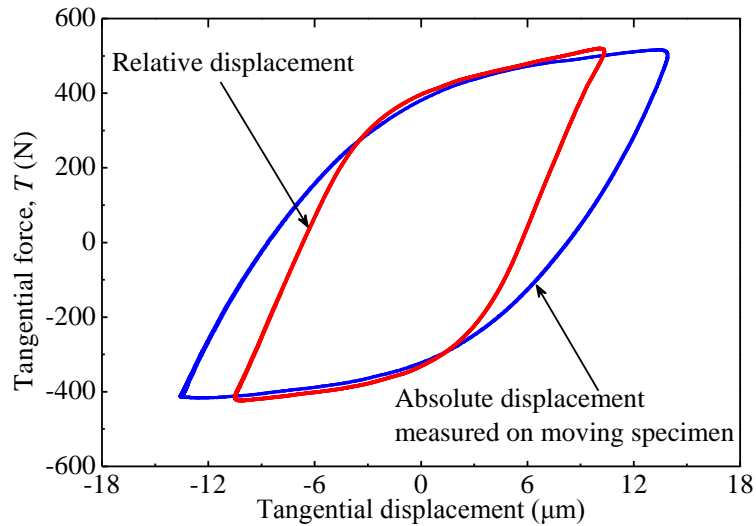


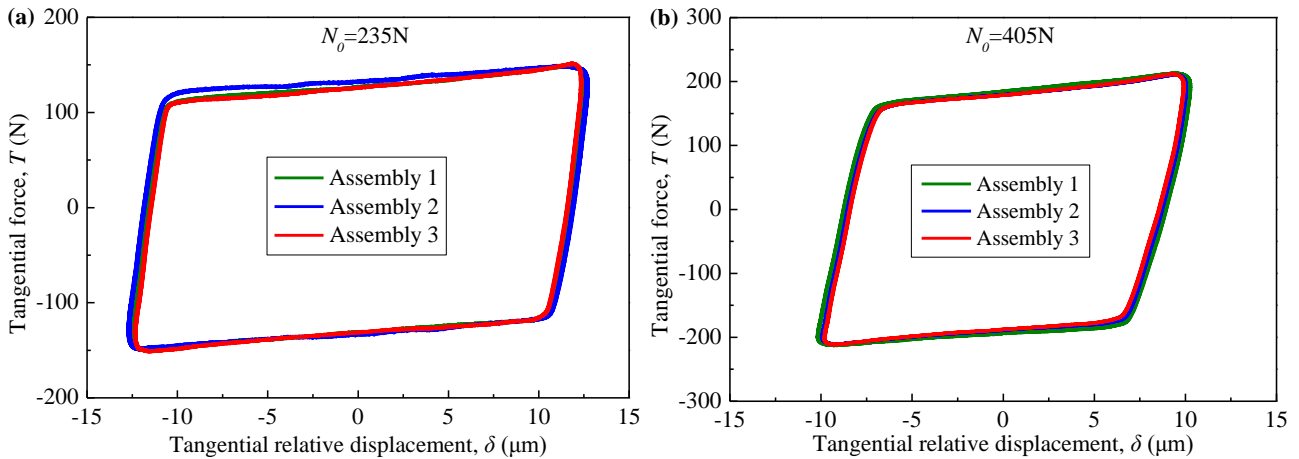
**Fig. 9.** Comparison of hysteresis loops based on relative displacement (the red one) and absolute displacement measured on the moving specimen (the blue one).

### 3.1 Repeatability tests

Two groups of tests ( $N_0=235$  N and 405 N) were performed to assess the repeatability of the measured loops and the estimated contact parameters. To this end, the same specimen pair was assembled, tested and disassembled three times. The measurement in each test lasted 1 sec, without any running-in time. Figure 10 shows the measured hysteresis loops under a sinusoidal excitation with amplitude 40  $\mu\text{m}$  and frequency 25 Hz. Each curve includes 25 periods. During this time, the change in the bolt preload was less than 0.5%. Comparing the loops of the three assemblies the degree of dispersion is very limited, indicating that the measurements are stable.

Table 1 lists the dissipated energy and contact parameters (contact stiffness and friction coefficient) obtained from the last measured hysteresis loops, the 25th. The dissipated energy is the area of the loop. The Coefficient of Variation (CV) was used to evaluate the influence of assembly uncertainty

288 on contact parameters and dissipated energy. The CV is a statistical measure of the dispersion of data  
 289 points in a data series around the mean and it is defined as the ratio of the standard deviation of  
 290 measured data to their mean. The results show that the CV of the friction coefficient and of the energy  
 291 dissipation was less than 4%, while the CV of the contact stiffness was slightly higher, but lower  
 292 than 5.5%. Therefore, the assembly uncertainty has less impact on the experimental results.



294 **Fig. 10.** Measured hysteresis loops under three different assemblies to evaluate the influence of  
 295 assembly uncertainty, (a)  $N_0=235$  N, (b)  $N_0=405$  N.

297 **Table 1.** Assessment of the repeatability of contact parameters and energy dissipation per cycle.

Contact parameters	Contact stiffness, N/ $\mu$ m		Friction coefficient		Energy dissipation, mJ	
	$N_0=235$ N	$N_0=405$ N	$N_0=235$ N	$N_0=405$ N	$N_0=235$ N	$N_0=405$ N
Assembly 1	155.3	155.1	0.549	0.467	6.06	6.73
Assembly 2	143.6	166.2	0.566	0.455	6.32	6.40
Assembly 3	158.4	171.3	0.548	0.453	5.99	6.29
Coefficient of variation	5.12%	5.04%	1.82%	1.65%	2.84%	3.54%

### 299 3.2 Effect of bolt preload

2  
3  
300 Tests were carried out to study the effect of bolt preloads on friction hysteresis. Figure 11(a) depicts  
4  
5  
6  
301 the measured hysteresis loops under five different bolt preloads forced with the same sinusoidal  
7  
8  
302 excitation (amplitude 25  $\mu\text{m}$ , frequency 25 Hz). It is seen that the influence of bolt preload on the  
9  
10  
11  
303 shape of the measured hysteresis loop is significant. As the bolt preload increases, the maximum  
12  
13  
14  
304 friction force gradually increases, and the sliding amplitude decreases.

15  
16  
17  
305  
18  
19  
20  
306 Figure 11(b) illustrates the tangential contact stiffness under different bolt preloads. The tangential  
21  
22  
23  
307 stiffness gradually increases with the bolt preload. This result is expected since the contact stiffness  
24  
25  
26  
308 depends, as a first approximation, on the contact area. This behavior is predicted by the Mindlin  
27  
28  
29  
309 theory [28], where the tangential contact stiffness increases with the radius of the contact area and  
30  
31  
32  
310 therefore with the normal load.

33  
34  
35  
311  
36  
37  
312 Figure 11(b) displays the friction coefficient as a function of the bolt preload. The gross-slip regime  
38  
39  
40  
313 could not be reached with preload greater than 902 N. Results show that the friction coefficient  
41  
42  
43  
314 increases with the preload. In [29] the friction coefficient was found depending on the preload as well.

44  
45  
46  
315 One explanation can be given considering that the friction coefficient is not only a material property  
47  
48  
49  
316 but depends both on material and on surface condition. The bolt preload changes the surface  
50  
51  
52  
317 morphology by smoothing the asperities. As the bolt preload increases, the change of the surface  
53  
54  
55  
318 morphology could give a different friction coefficient.

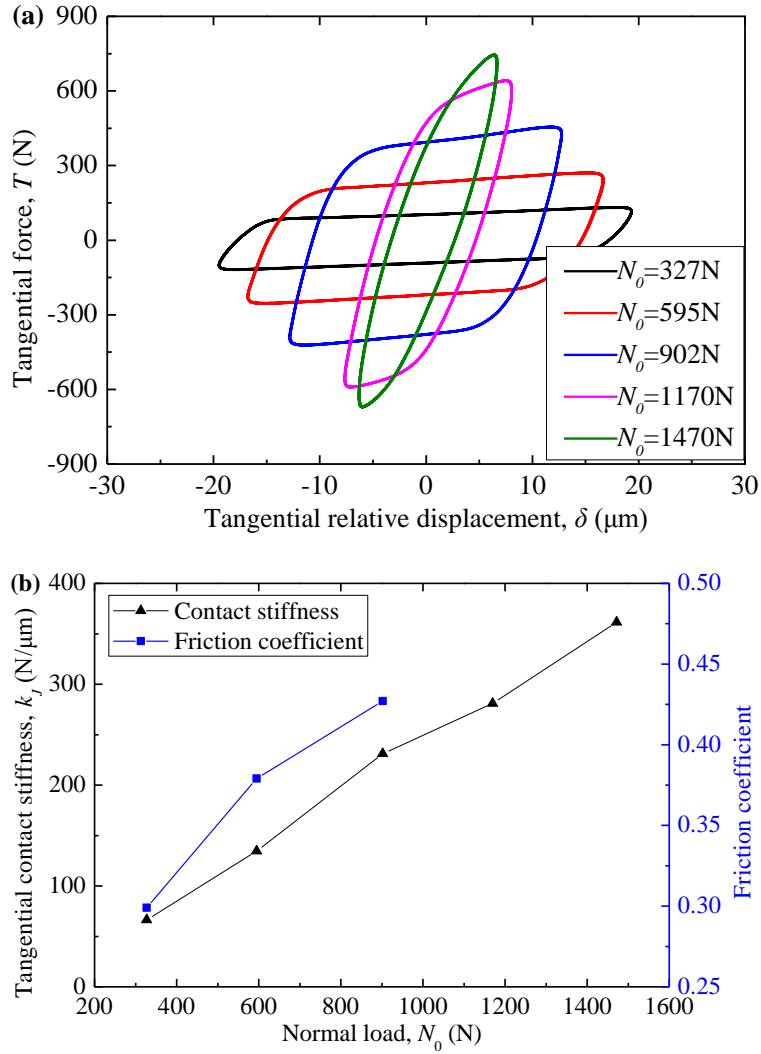


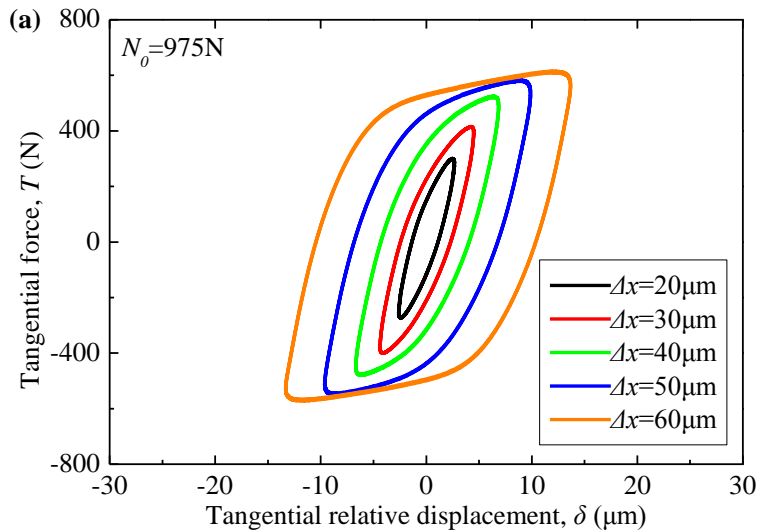
**Fig. 11.** Measured hysteresis loops and contact parameters under different bolt preloads: (a) measured hysteresis loops, (b) tangential contact stiffness and friction coefficient versus bolt preload.

### 3.3 Effect of excitation amplitude

Joints with constant bolt preload and different displacements were tested to study the effect of excitation amplitudes. After each test, the apparatus was disassembled and reassembled to set friction forces at the interfaces at zero and to ensure that the test conditions remained the same among the whole set of measurements. Figure 12(a) and (b) show the measured hysteresis loops as a function of the imposed displacement amplitude under two different preloads. The shape of the hysteresis loops

329 changed from elliptical to a parallelogram when increasing the imposed displacement amplitudes.  
 330 Two phenomena can be observed: (i) the tangential force increased almost linearly with the relative  
 331 displacement during the gross-slip phase and (ii) the tangential force increased suddenly at the end of  
 332 the gross-slip phase, as shown in Fig. 12(b).

333  
 334 The linear increase of the tangential force during the gross-slip phase was due to the elasticity of the  
 335 bolt shank. The bolt shank gives a “residual stiffness” whose origin and effect will be discussed in  
 336 detail in section 4. The sudden increase of the tangential force at the end of the gross-slip phase is due  
 337 to the bolt pinning effect. When the sliding distance was sufficiently large to exceed the gap between  
 338 the screw and the bolt hole, the screw was brought to contact with the bolt hole so that an ‘uplift’  
 339 appears. As the nominal gap between the screw and the bolt hole is 500  $\mu\text{m}$  (far larger than the  
 340 maximum sliding distance in Fig. 12(b)) the main reason for the uplift phenomenon is the assembly  
 341 uncertainty. The uplift was not found at the negative end of the hysteresis loops. Besides, the tangential  
 342 contact stiffness was not significantly sensitive to the excitation amplitude, as shown in Fig. 12(c).



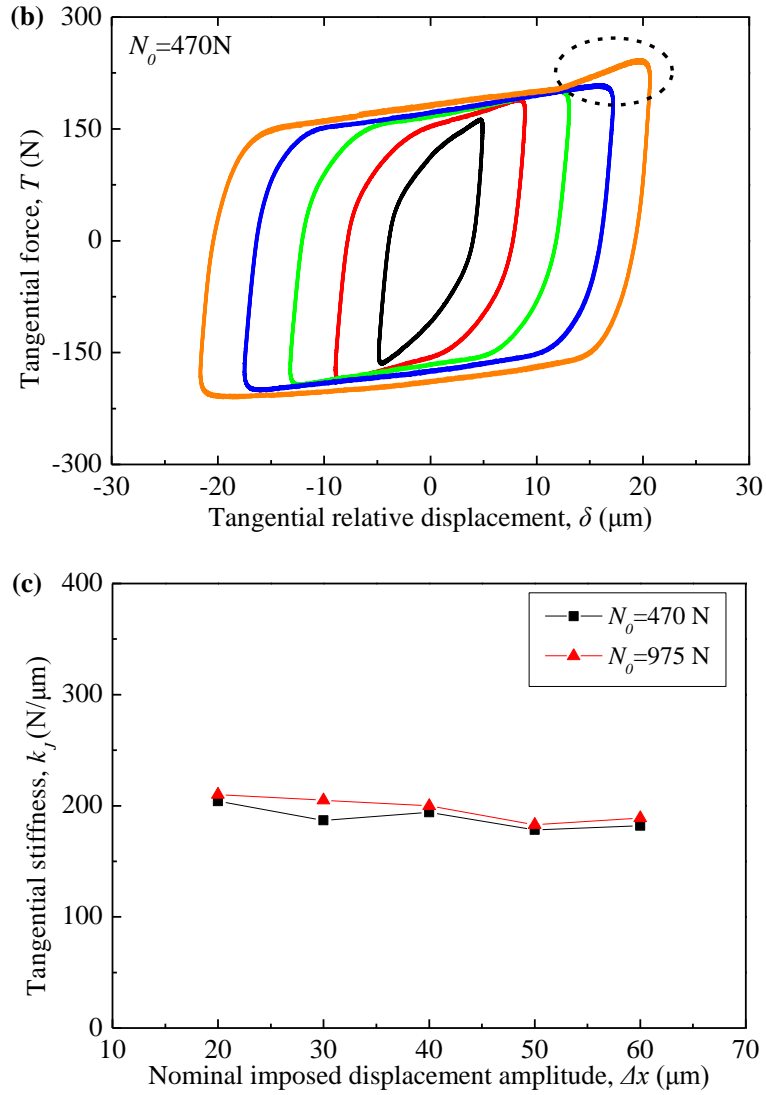
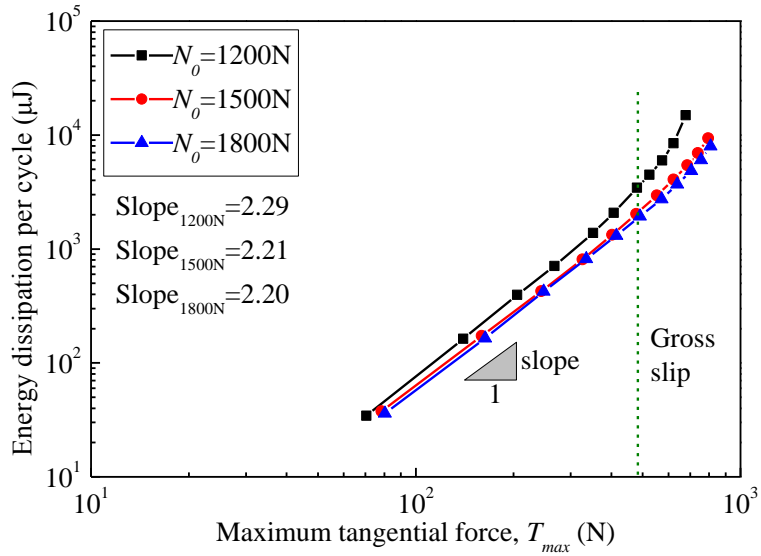


**Fig. 12.** Measured hysteresis loops under different nominal displacements imposed by the actuator: (a)  $N_0=975\ \text{N}$ , (b)  $N_0=470\ \text{N}$ , and (c) tangential stiffness versus imposed displacement amplitude.

Figure 13 shows the dissipated energy per cycle as a function of the maximum tangential load under three different bolt preloads (1200 N, 1500 N, and 1800 N). All data are plotted in a double logarithmic coordinate system. When the maximum tangential load is less than about 500 N, the dissipated energy shows a linear relationship with the maximum load whose slope is around 2.25. Within this load range, the interface does not undergo gross slip. The slope falls within the range of

354 2~3 as found in the literature [12, 29]. Besides, the energy/tangential force slope is not significantly  
 2  
 3  
 355 sensitive to the bolt preload.  
 4  
 5



356  
 24  
 357 **Fig. 13.** Energy dissipation per cycle versus maximum tangential force under different bolt preloads.  
 26  
 27

358  
 29  
 30  
 31  
 32  
 33  
 34  
 35  
 36  
 37  
 38  
 39  
 40  
 41  
 42  
 43  
 44  
 45  
 46  
 47  
 48  
 49  
 50  
 51  
 52  
 53  
 54  
 55  
 56  
 57  
 58  
 59  
 60  
 61  
 62  
 63  
 64  
 65

## 4 Extraction of contact parameters and measurement accuracy

The architecture of the fretting rig presented in this paper does not allow a direct measurement of the contact force  $F_{32}$  in Fig. 15 at the target interface. This architecture is common to many test rigs as those described in [11-17]. The force measured by the load cell depends on the contact forces at all the interfaces (between the screw head, the washer, the nut and the target interface) and on the elastic force in the bolt shank. Therefore, a numerical simulation is needed to correctly evaluate the force  $F_{32}$ . Two models, a finite element model and a simplified 5 dofs model, were used to determine the contact force  $F_{32}$  and its relationship with the measured tangential force  $T$ . Moreover, with these models, it is possible to set the proper correction to infer the contact stiffness  $k_t$  in the joint from the slopes measured on the hysteresis loops.

### 4.1 The finite element model

In the finite element model (see Fig. 14(a)) all components – bolt, washer, nut, fixed and moving specimens - were meshed using 8 nodes linear brick element with a 200 GPa modulus of elasticity and 0.3 Poisson's ratio. The model has 30448 nodes, 24693 elements, and 720 contact elements (only for the target contact interface). The mean area of the contact elements is  $0.50 \text{ mm}^2$ . The interaction between the contact surfaces was defined using the "Lagrange Multiplier" friction formulation with a friction coefficient  $\mu = 0.36$  as extracted from the experimental data. A quasi-static contact analysis was performed to simulate the load transfer on the joint. In the simulations, the moving specimen was displaced with an oscillating motion  $\delta$ . Both the amplitude of the oscillation,  $\delta=40 \text{ }\mu\text{m}$ , and the preload on the bolt,  $N_0=470 \text{ N}$ , were set as in the experimental tests.

379

2

380

5

381

8

382

10

383

13

384

16

385

19

386

22

23

387

37

388

54

389

56

390

59

60

61

62

63

64

65

Figure 14(b) illustrates the comparison between the measured and simulated results in terms of slopes of the hysteresis loop. The comparison shows that the simulated slopes both at the motion reversal, namely in the stick regime and during the slip regime are perfectly in agreement with their experimental counterparts. However, the hysteresis loop in Fig. 14(b) seems to indicate a non-Coulomb friction behavior of the joint. Nevertheless, an in-depth analysis of the system shows that this behavior is due to the chain of stiffness of the components that compose the joint than to a non-ideal friction contact.

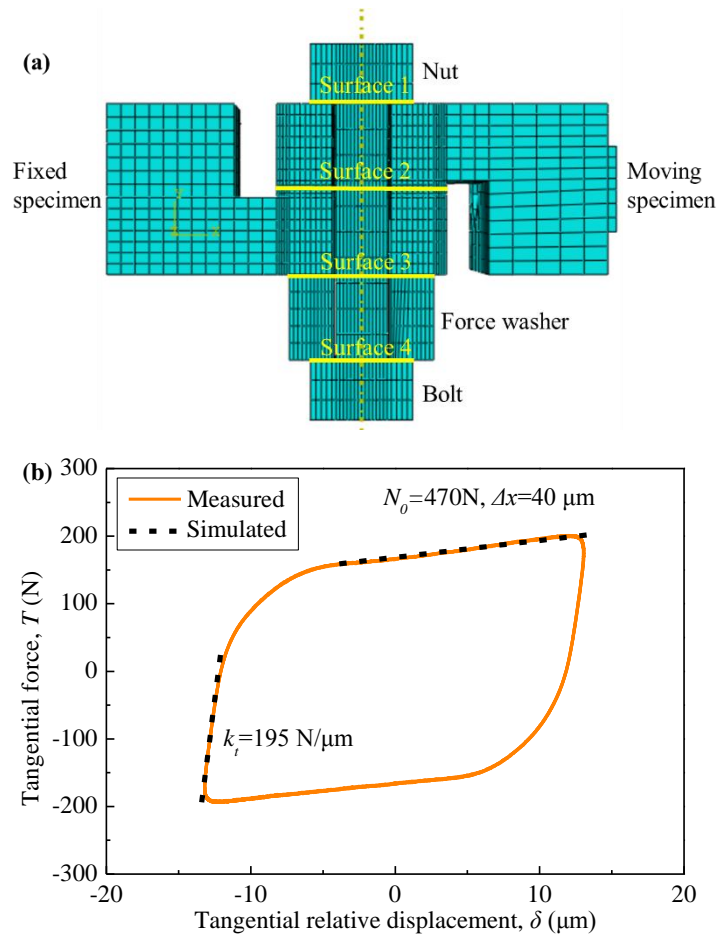


**Fig. 14.** (a) Finite element model with contact surfaces indicated by solid yellow lines. (b) comparison between the simulated slopes and the experimental counterpart.

391  
2  
3  
392  
4  
5  
393  
6  
7  
394  
8  
9  
10  
11  
12  
395  
13  
14  
15  
396  
16  
17  
18  
397  
19  
20  
21  
398  
22  
23  
24  
399  
25  
26  
400  
27  
28  
29  
401  
30  
31  
32  
402  
33  
34  
35  
36  
37  
403  
38  
39  
40  
404  
41  
42  
43  
405  
44  
45  
46  
406  
47  
48  
49  
50  
51  
52  
408  
53  
54  
55  
409  
56  
57  
58  
410  
59  
60  
61  
62  
63  
64  
65

## 4.2 Simplified model

The simplified model sketched in Fig. 15 helps in explaining the behavior of the joint. This model replaced the four contact surfaces - between the nut and the moving specimen, the washer and the fixed specimen, the bolt head and the washer in addition to the target contact surface - by an ideal Coulomb contact element. This contact element, in which micro-slip behavior was not considered, was composed by a linear spring and a slider. In this simplified model,  $k_1$ ,  $k_t$ ,  $k_3$ , and  $k_4$  are the contact stiffness parameters at the nut, at the target surface, at the washer and at the bolt head respectively;  $k_b$  is the stiffness between the bolt head and the nut. The stiffness parameter  $k_b$  was computed modelling the bolt shank as a beam. One end of the beam, the screw head, is clamped. The rotation of the other end, the nut, is constrained while is free to move in the transverse direction. The stiffness  $k_b$ , determined by the ratio between the transverse force in the clamp and the displacement of the nut, is

$$k_b = \frac{12E_s I_z}{(1 + \Phi)L_s^3}; \Phi = \frac{12E_s I_z}{GA_s L_s^2}. \quad (5)$$

In Eq. (5)  $L_s$ ,  $A_s$  and  $I_z$ , are the bolt shank length, the cross-section area and the second moment of area of the bolt shank respectively.  $E_s$  and  $G$  are the modulus of elasticity and the shear modulus of the material of the bolt. An analytical derivation of Eq. (5) is given in [31].

The finite element model of the joint was proved to be reliable in computing the contact stiffness  $k_j$ , as shown by a comparison between the simulation and the experimental measurement in Fig. 14. The same finite element model was used to determine the contact stiffness  $k_1$ ,  $k_t$ ,  $k_3$ , and  $k_4$ . These stiffnesses were calculated applying the bolt preload and a tangential force to the contact surface. The

411 ratio of the contact force with the induced displacement gave the contact stiffness. The results are  
 2  
 3  
 412 listed in [Table 2](#). [Figure 15\(b\)](#) depicts the stiffness between the fixed and moving specimens, namely  
 5  
 6  
 413 the points at which the relative displacement is measured. This figure clearly shows that the overall  
 7  
 8  
 414 stiffness  $k_J$  is the parallel of  $k_t$  with the series of  $k_1$ ,  $k_3$ ,  $k_4$ , and  $k_b$ , namely  $k_s$

$$k_s = \frac{k_1 k_3 k_4 k_b}{k_1 k_3 (k_4 + k_b) + k_4 k_b (k_1 + k_3)}. \quad (6)$$

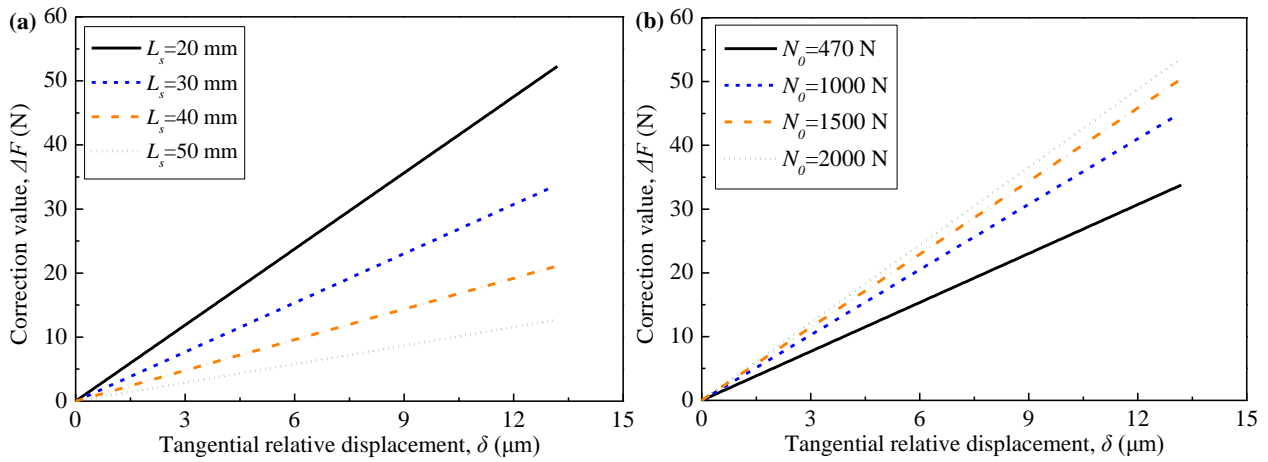
415 The contact stiffness of the joint  $k_t$  can be obtained by subtracting the stiffness series  $k_s$  from the  
 16  
 17  
 416 slope  $k_J$  derived from the hysteresis loop

$$k_t = k_J - k_s. \quad (7)$$

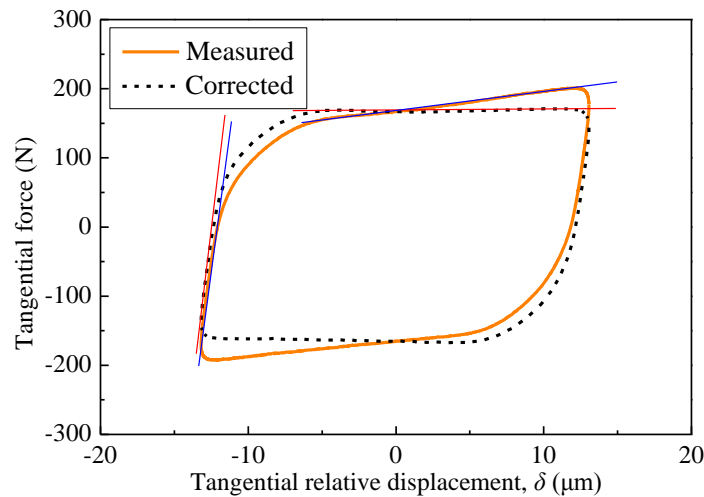
417 By using the simplified model described in **Appendix A**, it can be verified that when the contact at  
 25  
 26  
 418 the target interface slides the contact force at the other interfaces remains below the maximum  
 28  
 29  
 419 allowable friction force. The same value of the friction coefficient was assumed at all interfaces. In  
 30  
 31  
 420 this condition the stiffness  $k_t$  becomes zero while the other stiffness values remain at their nominal  
 33  
 34  
 421 value. The slope during the sliding regime, see the hysteresis loop in [Fig. 14\(b\)](#), was then the  
 36  
 37  
 422 stiffness  $k_s$  of the series to be used in Eq. (7) to determine the contact stiffness of the joint.



433 motion state of the target contact surface. Figure 16 illustrates the correction as a function of relative  
 2  
 3  
 434 displacement, of the length of the bolt shank and the bolt preload. The results show that the higher  
 5  
 6  
 435 the compliance of the bolt shank, the smaller the correction of the measured contact force. Figure 17  
 8  
 436 shows the comparison between the measured and the corrected hysteresis loops. The corrected  
 10  
 11  
 437 contact force remains constant during the gross-slip regime.



438  
 439 **Fig. 16.** The sensitivity of the correction parameter  $\Delta F$  to (a) the length of the bolt shank, (b) the  
 32  
 33  
 440 bolt preload.



441  
 442 **Fig. 17.** Comparison between the measured and the corrected hysteresis loops.

## 5 Conclusions

This paper presents a fretting apparatus to study friction hysteresis behavior in bolted joints.

Compared with similar test rigs proposed in the past, this rig has some unique features. An original arrangement of the prism allows measuring the relative displacements using only one laser beam.

Some rigs proposed in the past measured only the displacement of the moving surface, which was then assumed as the relative displacement. In more recent rigs the relative displacement was measured with two laser beams, increasing the cost and the complexity of the apparatus. From the mechanical point of view, this rig has been carefully designed to perform accurate measurements of the hysteresis loops. The rig exploits a closed-loop frame that makes the rig compact and with self-balanced action-reaction forces. A leaf spring guides the motion of the moving contact surface. All these details make the proposed rig a high precision device and make it unique among the rigs found in the literature so far.

Also, a simplified model to analyze the force transmission among the different interfaces was developed. In this model the contact interfaces were replaced by Jenkins contact elements. This model allowed discerning the origin of the residual stiffness in the gross-slip regime. It was found that the residual stiffness is due to the stiffness at the contact surfaces between the nut-bolt head, between the washer-bolt head together with the deformation of the bolt shank. A finite element model was developed to compute the contact stiffness at the joint interfaces while the stiffness of the bolt shank was computed with an analytical model. The residual stiffness operates during all the fretting regimes

464 activated during the tests, namely stick, microslip and gross-slip. Therefore, the contact stiffness at the  
2  
3  
465 target interface does not coincide with the slope of the hysteresis loop at the motion reversal.  
4  
5  
466 Consequently, a post-processing procedure to clean the slope from the residual stiffness and to extract  
6  
7  
467 the target interface stiffness from the measured hysteresis loops needs to be set up. This correction is  
8  
9  
10  
11  
128 small for slender shank, but it becomes significant when the bolt shank is squat. After this more  
13  
14  
159 detailed analysis, the measured target interface stiffness has been found in good agreement with the  
16  
17  
180 numerical calculation performed simulating the target contact surface with a finite element model.  
19  
20  
21  
22  
23  
24  
25  
26  
27  
28  
29  
30  
31  
32  
33  
34  
35  
36  
37  
38  
39  
40  
41  
42  
43  
44  
45  
46  
47  
48  
49  
50  
51  
52  
53  
54  
55  
56  
57  
58  
59  
60  
61  
62  
63  
64  
65

## Acknowledgments

472

2  
3

473

The authors wish to acknowledge and thank the China Science Challenge for funding their research

6

474

project (TZ2018007). Dongwu Li would also like to show his gratitude to China Scholarship Council

8

475

(CSC) for supporting him as a visiting Ph.D. to AERMEC lab of Politecnico di Torino within the

11

476

project EXTHENdED.

14

477

17

18

19

20

21

22

23

24

25

26

27

28

29

30

31

32

33

34

35

36

37

38

39

40

41

42

43

44

45

46

47

48

49

50

## Appendix A

The equilibrium equations in stick regime are given in Eq. (A.1). The displacement  $\delta$  is the displacement of the moving specimen while  $T$  is the force measured by the acquisition system. In the simplified model displacement of the fixed specimen is assumed null,  $u_3 = 0$ ,  $R$  being the reaction on the support.

$$\begin{bmatrix} k_b + k_1 & -k_1 & 0 & 0 & -k_b \\ -k_1 & k_1 + k_t & -k_t & 0 & 0 \\ 0 & -k_t & k_t + k_3 & -k_3 & 0 \\ 0 & 0 & -k_3 & k_3 + k_4 & -k_4 \\ -k_b & 0 & 0 & -k_4 & k_b + k_4 \end{bmatrix} \begin{Bmatrix} u_1 \\ \delta \\ u_3 \\ u_4 \\ u_5 \end{Bmatrix} = \begin{Bmatrix} 0 \\ T \\ -R \\ 0 \\ 0 \end{Bmatrix}. \quad (\text{A.1})$$

The equilibrium equations in slip regime are given in Eq. (A.2)

$$\begin{bmatrix} k_b + k_1 & -k_1 & 0 & 0 & -k_b \\ -k_1 & k_1 & 0 & 0 & 0 \\ 0 & 0 & +k_3 & -k_3 & 0 \\ 0 & 0 & -k_3 & k_3 + k_4 & -k_4 \\ -k_b & 0 & 0 & -k_4 & k_b + k_4 \end{bmatrix} \begin{Bmatrix} u_1 \\ \delta \\ u_3 \\ u_4 \\ u_5 \end{Bmatrix} = \begin{Bmatrix} 0 \\ T - \mu N \\ \mu N - R \\ 0 \\ 0 \end{Bmatrix}. \quad (\text{A.2})$$

The solution of Eq. (A.1) is

$$\begin{Bmatrix} u_1 \\ T \\ R \\ u_4 \\ u_5 \end{Bmatrix} = \frac{\delta}{k} \begin{Bmatrix} k_1(k_3k_4 + k_3k_b + k_4k_b) \\ k_1k_tk_3k_4 + k_1k_tk_3k_b + k_1k_tk_4k_b + k_1k_3k_4k_b + k_tk_3k_4k_b \\ k_1k_tk_3k_4 + k_1k_tk_3k_b + k_1k_tk_4k_b + k_1k_3k_4k_b + k_tk_3k_4k_b \\ k_1k_4k_b \\ k_1k_b(k_3 + k_4) \end{Bmatrix}. \quad (\text{A.3})$$

where  $k = k_1k_3k_4 + k_1k_3k_b + k_1k_4k_b + k_3k_4k_b$ .

The solution of Eq. (A.2) is

$$\begin{Bmatrix} u_1 \\ T \\ R \\ u_4 \\ u_5 \end{Bmatrix} = \frac{1}{k} \begin{Bmatrix} k_1\delta(k_3k_4 + k_3k_b + k_4k_b) \\ \mu Nk + k_1k_3k_4k_b\delta \\ \mu Nk + k_1k_3k_4k_b\delta \\ k_1k_4k_b\delta \\ k_1k_b(k_3 + k_4)\delta \end{Bmatrix}. \quad (\text{A.4})$$

## References

- [1] O. Vingsbo, S. Soderberg, On fretting maps, *Wear*, 1988, 126: 131–147. [https://doi.org/10.1016/0043-1648\(88\)90134-2](https://doi.org/10.1016/0043-1648(88)90134-2)
- [2] Gaul, L., Nitsche, R. The Role of Friction in Mechanical Joints. *ASME. Appl. Mech. Rev.* 2001, 54(2): 93–106. <https://doi.org/10.1115/1.3097294>
- [3] Iwan W D. A distributed-element model for hysteresis and its steady-state dynamic response. *Journal of Applied Mechanics*, 1966, 33(4): 893-900. <https://doi.org/10.1115/1.3625199>
- [4] Gaul L, Lenz J, Sachau D. Active Damping of Space Structures by Contact Pressure Control in Joints. *Journal of Structural Mechanics*, 1998, 26(1): 81-100. <https://doi.org/10.1080/08905459808945421>
- [5] Botto D, Lavella M. A numerical method to solve the normal and tangential contact problem of elastic bodies, 2015, *Wear*, 330-331: 629-635. <https://doi.org/10.1016/j.wear.2015.02.046>
- [6] Li D., Xu C., Liu T., et al. A modified IWAN model for microslip in the context of dampers for turbine blade dynamics. *Mech. Syst. Signal Process.*, 2019, 121: 14-30. <https://doi.org/10.1016/j.ymssp.2018.11.002>
- [7] Ungar E. E. The status of engineering knowledge concerning the damping of built-up structures. *Journal of sound and vibration*, 1973, 26(1): 141-154. [https://doi.org/10.1016/S0022-460X\(73\)80210-X](https://doi.org/10.1016/S0022-460X(73)80210-X)
- [8] Rogers P. F., Boothroyd G. Damping at metallic interfaces subjected to oscillating tangential loads, *J. Eng. Ind.* 1975, 97(3):1087-1093. <https://doi.org/10.1115/1.3438660>
- [9] Padmanabhan, K. K., Murty, A. S. R. Damping in Structural Joints Subjected to Tangential Loads. *Proceedings of the Institution of Mechanical Engineers, Part C: Mechanical Engineering Science*, 1991, 205(2), 121–129. [https://doi.org/10.1243/PIME\\_PROC\\_1991\\_205\\_099\\_02](https://doi.org/10.1243/PIME_PROC_1991_205_099_02)
- [10] Gaul L, Nackenhorst U, Willner K, et al. Nonlinear vibration damping of structures with bolted joints. *Proceedings-Spie the International Society for Optical Engineering*, 1994.
- [11] Gaul L, Lenz J. Nonlinear dynamics of structures assembled by bolted joints. *Acta Mechanica*, 1997, 125(1-4): 169-181. <https://doi.org/10.1007/BF01177306>
- [12] Ames, N. M., Lauffer, J. P., Jew, M. D., et al. Handbook on dynamics of jointed structures, No. SAND2009-4164. Sandia National Laboratories (2009). <https://doi.org/10.2172/1028891>
- [13] Abad J, Franco J M, Celorrio R, et al. Design of experiments and energy dissipation analysis for a contact mechanics 3D model of frictional bolted lap joints. *Advances in Engineering Software*, 2012, 45(1): 42-53. <https://doi.org/10.1016/j.advengsoft.2011.09.021>
- [14] Abad J, Medel F J, Franco J M. Determination of Valanis model parameters in a bolted lap joint: Experimental and numerical analyses of frictional dissipation. *International Journal of Mechanical Sciences*, 2014, 89: 289-298. <https://doi.org/10.1016/j.ijmecsci.2014.09.014>
- [15] Eriten M, Polycarpou A A, Bergman L A. Development of a lap joint fretting apparatus. *Experimental mechanics*, 2011, 51(8): 1405-1419. <https://doi.org/10.1007/s11340-010-9458-8>
- [16] Ouyang H, Oldfield M J, Mottershead J E. Experimental and theoretical studies of a bolted joint excited by a torsional dynamic load. *International Journal of Mechanical Sciences*, 2006, 48(12): 1447-1455. <https://doi.org/10.1016/j.ijmecsci.2006.07.015>

- 528 [17]Liu J, Ouyang H, Feng Z, et al. Dynamic behaviour of a bolted joint subjected to torsional  
529 excitation. Tribology International, 2019, 140: 105877. [https://doi.org/10.1016/j.triboint.2019.](https://doi.org/10.1016/j.triboint.2019.105877)  
530 [105877](https://doi.org/10.1016/j.triboint.2019.105877)
- 531 [18]Kartal M E, Mulvihill D M, Nowell D, et al. Determination of the frictional properties of titanium  
532 and nickel alloys using the digital image correlation method. Experimental Mechanics, 2011,  
533 51(3): 359-371. <https://doi.org/10.1007/s11340-010-9366-y>
- 534 [19]Schwingshackl C W, Petrov E P, Ewins D J. Measured and estimated friction interface parameters  
535 in a nonlinear dynamic analysis. Mechanical Systems and Signal Processing, 2012, 28: 574-584.  
536 <https://doi.org/10.1016/j.ymsp.2011.10.005>
- 537 [20]Schwingshackl C W. Measurement of friction contact parameters for nonlinear dynamic analysis.  
538 Topics in Modal Analysis I, Volume 5. Springer, New York, NY, 2012: 167-177. [https://doi.org/10.](https://doi.org/10.1007/978-1-4614-2425-3_16)  
539 [1007/978-1-4614-2425-3\\_16](https://doi.org/10.1007/978-1-4614-2425-3_16).
- 540 [21]Botto D, Lavella M. High temperature tribological study of cobalt-based coatings reinforced with  
541 different percentages of alumina, 2014, Wear, 318 (1-2): 89-97. [https://doi.org/10.1016/j.wear.](https://doi.org/10.1016/j.wear.2014.06.024)  
542 [2014.06.024](https://doi.org/10.1016/j.wear.2014.06.024)
- 543 [22]Botto D, Umer M, Gastaldi C, Gola M M. An experimental investigation of the dynamic of a blade  
544 with two under-platform dampers. Proceedings of the ASME Turbo Expo, 2017, 7B: Structures  
545 and Dynamics. <https://doi.org/10.1115/1.4037865>
- 546 [23]Umer M, Botto D. Measurement of contact parameters on under-platform dampers coupled with  
547 blade dynamics. International Journal of Mechanical Sciences, 2019, 159: 450-458.  
548 <https://doi.org/10.1016/j.ijmecsci.2019.06.010>
- 549 [24]Botto D, Umer M. A novel test rig to investigate under-platform damper dynamics. Mechanical  
550 Systems and Signal Processing, 2018. <https://doi.org/10.1016/j.ymsp.2017.07.046>
- 551 [25]Botto D, Campagna A, Lavella M, Gola M M. Experimental and numerical investigation of  
552 fretting wear at high temperature for aeronautical alloys. Proceedings of the ASME Turbo Expo,  
553 2010, 6. <https://doi.org/10.1115/GT2010-23356>
- 554 [26]Li Y, Hao Z, Feng J, et al. Investigation into discretization methods of the six-parameter Iwan  
555 model. Mechanical Systems and Signal Processing, 2017, 85: 98-110. [https://doi.org/10.1016/j.](https://doi.org/10.1016/j.ymsp.2016.07.032)  
556 [ymssp.2016.07.032](https://doi.org/10.1016/j.ymsp.2016.07.032)
- 557 [27]Brake, M. R. W. A reduced Iwan model that includes pinning for bolted joint  
558 mechanics. Nonlinear Dynamics, 2017, 87(2), 1335-1349.  
559 <https://doi.org/10.1007/s11071-016-3117-2>
- 560 [28]Mindlin R D, Mason W P, Osmer T F, et al. Effects of an oscillating tangential force on the contact  
561 surfaces of elastic spheres. Journal of Applied Mechanics-Transactions of the ASME, 1951, 18(3):  
562 331-331. [https://doi.org/10.1007/978-1-4613-8865-4\\_32](https://doi.org/10.1007/978-1-4613-8865-4_32)
- 563 [29]Eriten M, Polycarpou A A, Bergman L A. Effects of surface roughness and lubrication on the early  
564 stages of fretting of mechanical lap joints. Wear, 2011, 271(11-12): 2928-2939.
- 565 [30]Hartwigsen C. J., Song Y., McFarland D. M., et al. Experimental study of non-linear effects in a  
566 typical shear lap joint configuration. Journal of Sound and Vibration, 2004, 277(1-2): 327-351.  
567 <https://doi.org/10.1016/j.jsv.2003.09.018>
- 568 [31]Przemieniecki, J. S. Theory of matrix structural analysis. New York: McGraw-Hill, 1968.